Research Square

Preprints are preliminary reports that have not undergone peer review.
They should not be considered conclusive, used to inform clinical practice,
or referenced by the media as validated information.

Coordinated adaptive changes in insulin, insulin receptor, and inceptor genes in hystricognath rodents

Melisa E. Magallanes Alba
melisa.eliana.magallanes@gmail.com
Universidad de la República de Uruguay
Maite Hilario
Universidad de la República de Uruguay
Juan C. Opazo
Universidad San Sebastián
Enrique P. Lessa
Universidad de la República de Uruguay

Research Article

Keywords: Insulin axis, ELAPOR1, Exon skipping, Pseudogenization, Coevolution

Posted Date: August 20th, 2026

DOI: https://doi.org/10.21203/rs.3.rs-10656647/v1

License: This work is licensed under a Creative Commons Attribution 4.0 International License. Read Full License

Additional Declarations: No competing interests reported.

Abstract

Insulin is a master regulator of mammalian glycemia, yet hystricognath rodents exhibit highly divergent insulins with reduced biological activity. While selection on the hormone itself is well-documented, compensatory changes across the broader signaling axis remain largely unexplored. We identified signals of positive selection in *Insulin* (*ins*) and *ELAPOR1* (which encodes for Inceptor, a recently identified insulin regulator) within the hystricognath lineage. Positively selected sites of the insulin molecule were concentrated in the second binding site and in regions involved in hexamer formation. The adult insulin receptor isoform (*INSR-B*) exhibits structural remodeling across the broader hystricognath clade, driven by substitutions that neutralize the electrostatic charge of its binding pocket. In addition, comparative liver transcriptomics revealed striking lineage-specific compensations. The degu (*Octodon degus*) presents hepatic expression of *Ins* while retaining the canonical adult *INSR-B*isoform and basal *ELAPOR1* expression. The capybara (*Hydrochoerus hydrochaeris*) exhibits a complete absence of hepatic INSR-B, yet maintains strict tissue-specific restriction of *Ins* (no ectopy) and basal *ELAPOR1*. The guinea pig (*Cavia porcellus*) displays ectopic *Ins* overexpression, complete absence of *INSR-B*, and concurrent upregulation of *ELAPOR1*. Genomic interrogation across multiple caviomorph species traced this phenotypic progression to an ancestral regulatory silencing of exon 11 in the family *Caviidae*, which subsequently escalated to complete structural pseudogenization on the branch leading to the genus *Cavia*. This pseudogenization event is characterized by the loss of canonical splice donor sites and a single nucleotide deletion in the wild relative, *Cavia aperea*. Our results redefine the hystricognath insulin axis not only as divergent from the mammalian system, but as a unique evolutionary model in which a stepwise progression of regulatory silencing and lineage-specific exon pseudogenization has resulted in a radical restructuring of mammalian glucose homeostasis.

Introduction

Glycemic regulation in mammals is typically a conserved physiological system involving a network of hormones, growth factors, and receptors. Insulin, secreted by pancreatic β-cells, is a well-characterized hormone that lowers blood glucose levels, and its physiological properties are highly conserved across mammals (Jin Chan and Steiner 2000; Conlon 2001; De Meyts 2015; Rostène and De Meyts 2021). A notable exception to this strong sequence conservatism is found in hystricognath rodents (infraorder Hystricognathi, see (D'Elía et al. 2019)), a diverse group that includes Old World mole-rats (families Bathyergidae and Heterocephalidae), porcupines (Hystricidae), and several New World caviomorph families such as guinea pigs and capybaras (Caviidae), spiny rats (Echimyidae), chinchillas (Chinchillidae), and tuco-tucos (Ctenomyidae). Classic biochemical and structural studies established early on that insulins from this clade are not only highly divergent at the sequence level but also exhibit profound functional alterations. These include a loss of the ability to form zinc-coordinated hexamers and a drastically reduced biopotency, often retaining only 1% to 5% of the biological activity and receptor affinity of typical mammalian insulins (Blundell et al. 1971; Horuk et al. 1979; Bajaj et al. 1986; Opazo et al. 2005).

Given the evolutionary conservation of insulin in mammals (Conlon 2001), the discovery that insulin from guinea pigs (*Cavia porcellus*), degus (*Octodon degus*), and other hystricognaths exhibit unusual biological properties was unexpected. Early studies showed that guinea pig insulin and that of other hystricognath species were not neutralized by anti-bovine insulin antibodies (Davidson and Haist 1965; Davidson et al. 1968; Neville et al. 1973). Further experimental work demonstrated that hystricognath insulins exhibit reduced receptor-binding affinity (Zimmerman et al. 1974; Horuk et al. 1979; Bajaj et al. 1986) and lack the ability to form hexamers, the typical storage form of insulin in the β-cells of most mammals (Wood et al. 1975; Bajaj et al. 1986). These distinct physiological characteristics are at least partially attributable to differences in the primary structure of hystricognath insulins (Bajaj et al. 1986; Opazo et al. 2005). Despite these divergent features, hystricognaths can maintain glycemic homeostasis (Opazo et al. 2004), albeit with elevated circulating insulin levels that likely compensate for reduced biological activity. The delicate nature of this compensatory mechanism is evidenced by species like the degu, which are highly susceptible to spontaneous diabetes when their natural environment or diet is altered (Opazo et al. 2004; Edwards 2009). Interestingly, their proinsulins also show enhanced mitogenic activity and interact with additional growth receptors (King and Kahn 1981; King et al. 1983).

Opazo et al. (2005) identified codons in the insulin gene of caviomorph rodents that have evolved under positive selection, likely contributing to their distinct insulin properties. These molecular changes affect the second binding site, essential for insulin-receptor interaction (De Meyts 2015; Lawrence 2021; Choi and Bai 2023), and may also alter regions involved in insulin-insulin interactions, potentially explaining the inability to form hexamers. Adding to the picture of divergence of hystricognaths (Irwin 2020), reported accelerated amino acid substitution rates in both the insulin receptor (*Insr*) and the glucagon (*Gcg*) genes in hystricognaths, suggesting broader evolutionary changes across the glycemic regulation axis in this group. Reinforcing this view, a genome-wide scan

detected robust signals of adaptive evolution specifically tailored to the insulin and insulin-like growth factor (Igf) signaling pathways in the giant capybara (*Hydrochoerus hydrochaeris*), linking these alterations to growth and metabolic tradeoffs (Herrera-Álvarez et al. 2021). In most mammals, the metabolic action of this axis is heavily dependent on the alternative splicing of *Insr*. The retention of exon 11 generates the adult metabolic isoform (*INSR-B*). In contrast, its exclusion yields the embryonic isoform (*INSR-A*), which exhibits higher promiscuity and affinity for proinsulin and insulin-like growth factor 2 (Igf2) (Belfiore et al. 2009). The alternatively spliced exon 11 encodes a 12 amino acid segment (residues 717–728) of the alpha subunit of the receptor that disrupts binding to Igf2 (Frasca et al. 1999). How this structural plasticity operates in hystricognaths remains unknown.

A recent addition to our understanding of glycemic regulation is the protein Inceptor (insulin receptor regulator), encoded by the gene *ELAPOR1* (Endosome-Lysosome Associated Apoptosis and Autophagy Regulator 1). This protein plays a key role in insulin signaling in pancreatic β-cells (Ansarullah et al. 2021). Inceptor interacts with the insulin and Igf1 receptors at the cell membrane to promote clathrin-mediated endocytosis, thereby reducing β-cell responsiveness to insulin. More recently, Siehler et al. (2024) showed that Inceptor also acts as a sorting receptor in the cytoplasm, directing insulin and proinsulin toward lysosomal degradation. While much remains to be learned about this protein, its discovery opens new avenues for understanding insulin regulation in pancreatic β-cells (Burchfield and James 2021; Hall and Choi 2021) and potentially in other tissues (Bilekova et al. 2023). Given the unique insulin biology of hystricognath rodents, it is plausible that Inceptor may also have undergone lineage-specific modifications.

Building on documented interactions among insulin, Insulin receptor, Igf1 receptor, and Inceptor, we hypothesized that the entire glycemic signaling axis has undergone a systemic, co-evolutionary restructuring in hystricognath rodents. Because evolutionary adaptation frequently encompasses not only sequence divergence but also transcriptomic rewiring (Verta and Jacobs 2022), we postulated that changes in tissue-specific gene expression and alternative splicing might play a key compensatory role. To test this, we employed a multi-tiered approach encompassing molecular evolution models, multi-dataset transcriptomics, comparative phylogenomics, and 3D structural modeling. Our maximum likelihood analyses show a signature of positive selection on *Ins* and *ELAPOR1*. Analyses of selection in *Insr* are equivocal. However, comparative transcriptomics reveals striking lineage-specific physiological compensations across the hystricognath radiation. While the degu (*Octodon degus*) presents a moderate divergence from the canonical mammalian pattern (exhibiting mild hepatic *Ins* ectopy while retaining a functional adult *INSR-B* isoform), members of the family *Caviidae* exhibit a complete transcriptomic shift toward the embryonic *INSR-A* isoform. Within this family, the capybara (*Hydrochoerus hydrochaeris*) shows an intermediate phenotype: its liver completely lacks *INSR-B* expression, yet it maintains strict tissue-specific restriction of insulin (no hepatic ectopy) and basal *ELAPOR1* levels. In contrast, the guinea pig (*Cavia porcellus*) exhibits ectopic overexpression of both *Ins* and *ELAPOR1*. Through high-resolution genomic interrogation, we traced these differences to a stepwise mutational degradation of exon 11 within Caviidae. While functional exclusion in the capybara is driven by the accumulation of exonic splicing silencer (ESS) motifs, advanced pseudogenization is fixed in the genus *Cavia*, where the complete loss of the canonical 'GT' splice donor site physically blinds the spliceosome. Taken together, these genomic and transcriptomic profiles demonstrate that the regulatory silencing of the adult metabolic receptor was an ancestral event in Caviidae, which later resulted in the unique, multi-tiered physiological compensation exclusive to the *Cavia* lineage.

Materials and methods

DNA sequences

To assemble a comprehensive dataset of coding sequences (CDS) for insulin (*Ins*), insulin receptor (*Insr*), insulin-like growth factor 1 receptor (*Igf1r*), and *ELAPOR1*, a hierarchical sequence retrieval and annotation strategy was implemented across a broad representation of rodent lineages.

First, we prioritized annotations from the NCBI RefSeq database (Sayers et al. 2022). For species with available RefSeq records, the corresponding CDS for the genes of interest were downloaded directly using the NCBI Datasets command-line tools (O'Leary et al. 2024). Second, for species lacking RefSeq annotations but possessing whole-genome assemblies, we performed automated similarity-based annotations using miniprot v0.18 (Li 2023) with *Mus musculus* protein sequences as queries. The corresponding CDS were extracted using gffread v0.12.7 (Pertea and Pertea 2020). Because miniprot aligns protein queries to genome assemblies while preserving exon–intron boundaries, we retained only the top-scoring hit per genome to ensure orthology. To corroborate the orthology of all retrieved sequences and rule out potential paralogs, we subsequently constructed a preliminary Neighbor-Joining (NJ) phylogenetic tree as an additional validation step.

Third, when automated annotation failed to recover reliable CDS, often due to highly fragmented genome assemblies, we performed manual annotations using whole-genome sequencing (WGS) contigs. Finally, for phylogenetically critical taxa lacking genomic data, we leveraged available raw RNA-seq datasets from the Sequence Read Archive (SRA) to perform *de novo* transcriptome assemblies using SPAdes v4.2.0 (Prjibelski et al. 2020), enabling the successful recovery of the target transcripts. This approach was specifically applied to recover the target transcripts for *Cuniculus paca* (BioProject: PRJNA788430) and three species of tuco-tucos: *Ctenomys pearsoni*, *C. rionegrensis*, and *C. torquatus* (BioProject: PRJNA817291).

All retrieved sequences were subjected to stringent quality filters to discard those with unexpected lengths or internal stop codons, and the presence of conserved functional domains was verified. This multi-tiered strategy ensured the inclusion of critical taxa for phylogenetic and comparative analyses while maintaining strict standards for sequence quality and orthology. Our sampling encompassed representative species from all major lineages of hystricomorph rodents, including bathyergids, heterocephalids, hystricids, caviids, octodontids, chinchillids, and erethizontids. Additionally, we included the sister group to hystricognaths (ctenodactylids), as well as non-hystricomorph rodents (supramyomorphs and sciuromorphs) and selected placental mammals, such as lagomorphs and primates (**Table S1**).

Coding sequence alignments were generated using MACSE (Ranwez et al. 2021), which accounts for underlying codon structures, with manual adjustments applied as necessary. To establish the evolutionary framework, a sample of 1000 species-level phylogenetic trees for mammals was downloaded from VertLife (https://vertlife.org/data/mammals) for the species included in each dataset. These trees were inferred using a Bayesian framework integrating molecular sequence data and taxonomic constraints (Upham et al. 2019), and replicate trees reflect phylogenetic uncertainty in the evolutionary history of Mammalia. Their respective consensus trees were generated with the ape package v5.8 (Paradis and Schliep 2019). All annotation and filtering steps were carried out using our reproducible pipeline, which is publicly available at https://github.com/Melisa-Magallanes/evoseqaligner.

Natural selection analysis

We used CODEML, implemented in PAML v4.10.10 (Yang 2007), to test for variation in selective regimes, including positive selection, across genes in hystricognath rodents. Specifically, we applied branch models to estimate ω values (the ratio of nonsynonymous to synonymous substitutions) under three alternative scenarios. For each gene, the following models were fitted: 1) null model **(1ω)**: a single nonsynonymous/synonymous rate ratio ($\omega = d_N/d_S$) for all branches; two-rate models **(2ω)**: one ω for hystricognath rodents (as a total group) and another for all remaining branches; 3) three-rate model **(3ω)**: separate ω ratios were assigned to (i) caviomorph rodents, (ii) other non-caviomorph hystricognath rodents, and (iii) all other branches.

To ensure convergence, each model was run four times with different initial ω values (0.5, 1, 2, and 3). Likelihood ratio tests (LRTs) were used to compare models with different numbers of ω-values. Statistical significance of the LRTs was calculated in R using the pchisq function.

This strategy allowed us to detect whether elevated ω values, when statistically supported, reflected an overall acceleration in hystricognath rodents. If so, we further examined whether a separate ω was warranted for the caviomorph lineage. We also used site models to further examine the role of natural selection in shaping the evolution of our genes of interest. Specifically, we implemented models M7 and M8 in CODEML (Yang 2007) solely on the hystricognath data and subtree, and compared them using LRTs. A significant LRT supported the inclusion of a class of sites with $\omega > 1$, which is permitted in M8 but not in M7. We applied Bayes Empirical Bayes (BEB) analysis to identify specific codon sites that may be evolving under positive selection. As with the branch models, each site model was run 4 times with different initial ω values (0.5, 1, 2, and 3) to assess convergence.

For each locus, codons identified as potentially being under positive selection were mapped onto the primary structure of the reference transcript to assess their distribution across functional domains. To visualize their spatial context, we used ChimeraX v1.10.1 (Meng et al. 2023) to map these sites onto the following three-dimensional protein structures: preproinsulin (P01308 · INS_HUMAN), insulin (PDB6O17 · INS_HUMAN), insulin receptor preprotein (P06213 · INSR_HUMAN), the insulin receptor ectodomain (EMDB: EMD-10273), and ELAPOR1 (ELAPOR1; Q6UXG2).

Transcriptomic Data Retrieval and Isoform Quantification

To evaluate the expression dynamics of the glycemic signaling axis, we analyzed publicly available RNA-seq datasets encompassing different developmental states. Two independent BioProjects were retrieved from the Sequence Read Archive (SRA): (i) hepatic expression (PRJNA788430, (Lu et al. 2022)), including samples from *Mus musculus*, *Rattus rattus*, *Hydrochoerus hydrochaeris*, *Cavia porcellus*, and *Octodon degus*; and (ii) ontogenetic transition comparing fetal and maternal liver from *C. porcellus* (PRJNA1373124; (Hasan et al. 2025)) (**Table S2**). To specifically assess the stoichiometric relationship and relative transcriptional dynamics among the core components of the glycemic signaling axis, a targeted pseudoalignment strategy was implemented. A custom reference index was built using only the annotated coding sequences of *Ins*, *Insr* (isoforms A and B), and *ELAPOR1*. Transcript quantification was performed using kallisto (Bray et al. 2016). Because the quantification space was restricted to this highly specific panel, expression levels are reported as targeted Transcripts Per Million (tTPM). This metric represents the relative abundance and transcriptional fraction of each gene strictly within the isolated network, rather than its expression relative to the global transcriptome. Additionally, splice-aware alignments were generated with HISAT2 (Kim et al. 2015) and visually inspected in the Integrative Genomics Viewer (IGV) (Robinson et al. 2011) to confirm exon coverage and validate the structural absence of the *INSR-B* isoform.

Genomic Exploration and Splice Site Interrogation

Isoforms of INSR differ in their exclusion (INSR-A) or inclusion (INSR-B) of exon 11 in processed mRNA (Seino and Bell 1989). To trace the evolutionary origin of the exon 11 exclusion, we designed a high-resolution comparative phylogenomics pipeline across hystricognath species (**Table S3**). Initially, a tBLASTn search was performed against whole-genome sequence (WGS) assemblies using the amino acid sequence of *Mus musculus* INSR (spanning exons 10 to 12) as a query to identify the general genomic neighborhood. The contig/scaffold containing the alignment was downloaded.

To precisely delimit the locus, we executed miniprot (Li 2023) on the downloaded sequences using *M. musculus* exon 10 and exon 12 sequences as independent anchors. Genomic coordinates were extracted from the resulting GFF files, enabling computational cropping of the specific intronic region containing the alternative exon. The length of the cropped loci was compared across species to rule out large-scale chromosomal deletions (**Table S**4).

To identify highly divergent or pseudogenized remnants of exon 11, we utilized the heuristic aligner Exonerate v2.4.0 (Slater and Birney 2005) in the protein2genome model. A diverse panel of mammalian exon 11 sequences was used as baits to ensure alignments in regions with non-canonical splice sites. For each species, the hit with the highest bit-score was selected. The putative exon, along with 15 base pairs of flanking intronic sequences at both the 5' and 3' ends, was extracted for manual inspection of the integrity of the canonical splice acceptor (AG) and donor (GT) dinucleotides, and to detect lethal indels that result in reading frame shifts.

Protein Structure Prediction and Conformational Modeling

To assess the structural consequences of adaptive mutations in the hystricognath receptor, we selected the tuco-tuco (*Ctenomys rionegrensis*) as a representative model of lineages that maintain a transcriptionally functional, yet highly divergent, *INSR-B* isoform. This choice allowed for a direct, homologous structural comparison against the canonical human receptor monomer. The 3D structure was predicted using AlphaFold3 (Abramson et al. 2024). The generated model was imported into UCSF ChimeraX v1.10 (Meng et al. 2023) to perform a conformational superposition against the experimentally determined structure of the canonical human INSR-B (6SOF). This comparative modeling allowed us to evaluate spatial torsions, local domain shifts, and the specific structural plasticity required by the hystricognath receptor to accommodate its highly divergent insulin ligand, with a particular focus on regions identified as potentially under positive selection.

Results

Variation in ω across taxa

The taxa and tree used for the analysis of positive selection in each focal gene are presented in **Fig. 1**. Replicate runs of both branch and site models, starting with different ω values, consistently converged to highly similar results. For instance, log-likelihood (lnL) values across replicates were similar to the fifth decimal place.

For *Ins*, the two-rate model (separate ω for hystricognath rodents versus all other mammals) was the model that had the better fit (**Table 1**). In contrast, in the case of the *Igf1r*, none of the more complex models had a better fit in comparison to the one omega model (**Table 1**). Finally, for *Insr* and *Elapor1*, the three-ω model, estimating distinct ratios for the background, non-caviomorph hystricognath, and caviomorph lineages, provides a better fit (**Table 1**). However, in contrast to an expectation of a progressive increase toward the caviomorph clade, ω estimates for caviomorph and other hystricognath lineages were of similar magnitude, both clearly higher than those of background branches (Fig. 2; **Table 1**). This pattern indicates an overall acceleration of nonsynonymous substitution rates across the hystricognath radiation rather than a further intensification restricted to caviomorph rodents (Fig. 2).

Elevated ω values in certain lineages, as estimated using branch models, suggest changes in selective regimes, including, but not restricted to positive selection. For this reason, site models M7 and M8 were used to further investigate the elevated ω values observed in *Ins*, *Insr*, and *ELAPOR1*. These analyses were conducted on datasets restricted to hystricognath rodents, focusing only on genes for which the two- or three-omega models provided a better fit (i.e., *Ins*, *Insr*, and *ELAPOR1*). Consequently, site models were not applied to *Igf1r*, as no significant difference in ω across taxa was detected in the branch models for this gene.

For all three genes, M8 models provided a significantly better fit than M7 models, with $p < 0.036$ for *Ins* and $p < 0.00001$ for both *Insr* and *ELAPOR1*. The Bayes Empirical Bayes (BEB) analysis revealed variation in both the estimated ω values and the proportion of codon sites inferred to be under positive selection. Specifically, 2.8% and 2.31% of sites were assigned to the positively selected class in *Ins* (ω = 3.09) *and ELAPOR1* (ω = 1.695), respectively. In the case of *Insr*, however, ω = 1 was obtained for a class comprising 3.37% of the sites. The location and, when possible, functional significance of the sites are presented below, with emphasis on sites with strong posterior probability support (**Table 1**).

Location of sites under positive selection in the protein structures

Using site models, we identified four codon sites in the *Ins* gene assigned to the positively selected class (ω > 1). Among these, site B22 exhibited the strongest Bayes Empirical Bayes (BEB) posterior probability support (PP = 0.971). Three additional sites, A13 (PP = 0.619), B17 (PP = 0.673), and B27 (PP = 0.928), also clustered within this class with moderate support. Our findings are largely congruent with previous studies focused specifically on caviomorphs (Opazo et al. 2005), which similarly identified A13 and B17 as targets of adaptive evolution. When mapped onto the three-dimensional structure of mature insulin (Fig. 3), A13, B17, and B22 localize in close spatial proximity on the protein surface. Functionally, these residues constitute key components of the second binding site, which is critical for insulin-receptor interaction, and are equally essential for the formation of insulin hexamers, the standard storage conformation in mammalian beta-cells (De Meyts 2015; Gutmann et al. 2020a; Lawrence 2021). Furthermore, while site B27 is not directly adjacent to this primary cluster, it immediately flanks the highly conserved "aromatic triplet" (B24–B26), a structural motif indispensable for hexamerization and receptor binding in canonical mammals (Weiss and Lawrence 2018).

Insr presents seemingly conflicting results of the sites models. On the one hand, there is strong support for M8 over M7 ($p < 0.00001$). However, the additional class of sites is fit to a value of ω = 1, which may be explained by relaxation of negative selection and strictly neutral evolution of that class of sites. That said, it is worth noting that several of the identified residues with PP > 1 (e.g., positions 508S, 509F, 565L, 568N, and 572S, based on human INSR numbering) map directly to the structural region defined as "Site 2", which mediates the interaction with the secondary binding surface of the insulin molecule (Gutmann et al. 2020b). Remarkably, examining the point-to-point intermolecular contacts reported by Gutmann et al. (2020) reveals a direct spatial correspondence between the selected sites in the receptor and those previously identified in the hystricognath insulin ligand. For instance, insulin site A13 interacts directly with receptor position 565L (PP = 0.946). Similarly, insulin site B17 forms strong physical contacts with receptor sites 508S and 509F.

In *ELAPOR1*, sites assigned to the positively selected class (ω > 1) are restricted to the ectodomain of the protein (**Figure S1**). Several residues (6H, 13R, 18T, and 40Q) are located within the signal peptide, suggesting lineage-specific modifications that might influence receptor targeting and processing in the secretory pathway. Among these, position 40Q exhibits strong posterior probability support (PP = 0.951). A second broad cluster of selected sites falls within the first and second cysteine-rich domains (C1-C2). While several positions in this region show moderate support (e.g., 148A, 156S, 238R, 254K, and 313P), strong statistical evidence (PP > 0.95) is localized specifically to residues 364L (PP = 0.957) and 378H (PP = 0.988). Further along the ectodomain, another notable concentration of possibly selected sites occurs at the boundary between the C2 and the mannose-6-phosphate receptor (M6P) regions. This includes residue 639V, which displays one of the highest posterior probabilities in the entire gene (PP = 0.988), alongside

moderately supported neighboring sites such as 662R (PP = 0.932), 660F, 663N, and 670N. An additional moderately supported site (825T) lies closer to the C-terminus of the ectodomain.

This broad distribution of positively selected residues indicates that adaptive evolution in *ELAPOR1* is not confined to a single structural domain. Instead, changes in the signal peptide and cysteine-rich regions may affect its trafficking or its physical interaction with the insulin receptor at the plasma membrane. Concurrently, substitutions at the C2–M6P boundary might influence ligand sorting or endocytic regulation. Overall, these results strongly support the hypothesis that *ELAPOR1* has undergone significant adaptive diversification in hystricognath rodents. This structural evolution possibly serves as an integrated compensatory mechanism that modulates the internalization and degradation of their highly divergent insulin and proinsulin molecules within β-cells, a hypothesis that should be tested experimentally.

Transcriptomic exploration

To determine whether the evolutionary divergence detected by the sequence analyses is associated with alterations in gene expression *in vivo*, we analyzed publicly available RNA-seq datasets. Given that the liver is the primary target organ for insulin clearance and metabolic action, hepatic transcriptomes were used.

- Hepatic expression divergence

To evaluate these divergences *in vivo*, adult hepatic transcriptomes were analyzed by comparing two murine rodents (*M. musculus*, *R. rattus*) against three caviomorphs (*C. porcellus*, *O. degus, and H. hydrochaeris*). This analysis revealed striking lineage-specific patterns within the insulin axis (Fig. 4A). While murine rodents restrict *Ins* transcription to pancreatic beta-cells (with negligible hepatic levels) (Melloul et al. 2002; Tabula Muris Consortium et al. 2018) and rely almost entirely on the adult INSR-B isoform, the caviomorph species exhibit divergent transcriptomic architectures.

The degu presents a moderate divergence from the murine pattern. While it exhibits mild hepatic *Ins* ectopic expression and upregulates *INSR-A*, it crucially maintains expression of a functional adult *INSR-B* isoform and keeps *ELAPOR1* at basal levels.

In contrast, members of the family Caviidae (*Hydrochoerus* and *Cavia*) share a complete loss of the adult *INSR-B* isoform, relying exclusively on the embryonic *INSR-A* in the adult liver. However, their subsequent compensatory strategies diverge radically. The capybara (*Hydrochoerus hydrochaeris*) accommodates this receptor shift without triggering broader transcriptomic alterations; it maintains strict tissue-specific restriction of *Ins* (no hepatic ectopy) alongside basal *ELAPOR1* expression. In contrast, the guinea pig exhibits ectopic *Ins* expression in the adult liver, likely to circumvent the reduced biological activity of the mutated hormone by synthesizing it directly at the primary target tissue. In this context, the concurrent massive upregulation of *ELAPOR1* may serve as a homeostatic "emergency brake" to protect the hepatic tissue from receptor desensitization or cellular toxicity driven by local insulin overexposure.

Together, these profiles demonstrate that rather than relying on a single shared trait, hystricognath rodents evolved a highly variable, step-wise repertoire of transcriptomic strategies to cope with the historical divergence of their insulin signaling axis. Additional transcriptomic studies are needed to further explore this variation among other hystricognath lineages.

● Absence of Ontogenetic Splicing Transition

To assess whether these divergent splicing patterns are established during development or represent a loss of adult plasticity, paired fetal and maternal liver transcriptomes in the guinea pig were analyzed. In most mammals, the liver undergoes a postnatal alternative splicing switch, transitioning from INSR-A to INSR-B (Seino and Bell 1989; Frasca et al. 1999; Belfiore et al. 2009). However, our analysis revealed a complete retention of the embryonic state in the guinea pig (Fig. 4B). Both fetal and maternal livers exhibited statistically identical, high *INSR-A* expression levels (Wilcoxon test, p = 0.82), confirming the constitutive reliance on this isoform. Similarly, the expression of the compensatory receptor *ELAPOR* remained high across both stages (p = 0.82). Strikingly, while ectopic *Ins* expression was remarkably high in the adult liver (Fig. 4A), it was entirely repressed in both the fetal and maternal conditions (Fig. 4B). This might suggest that hepatic insulin ectopy is a phenotypically plastic trait rather than a constitutive one. We hypothesize that this ectopic expression is silenced during pregnancy to facilitate the physiological insulin resistance required for fetal nutrition (Haig 1993; Barbour et al. 2007; Napso et al. 2018).

Validation of Insr Exon 11 Loss in Caviidae

To empirically rule out cryptic transcription at levels undetectable by standard pseudoalignment, the physical mapping of raw RNA-seq reads across the guinea pig *INSR* locus was analyzed for both the guinea pig and the capybara. Visual exploration of these alignments revealed a consistent structural pattern across all evaluated datasets. In the guinea pig, and the capybara, there was an absolute absence of reads mapping to the genomic region corresponding to exon 11 (Fig. 5A). Sashimi plots physically confirmed an unbroken, clean splice junction jumping directly from the 3' boundary of exon 10 to the 5' boundary of exon 12. This physical evidence corroborates the finding that hepatic *INSR-B* expression is nonexistent, thereby placing the entirety of metabolic signaling demands on the embryonic *INSR-A* isoform.

Ancestral Loss of the Adult INSR-B Isoform in the Caviidae Lineage

To determine whether this transcriptomic exclusion is exclusive to the guinea pig or represents a deeper ancestral event, we interrogated the high-resolution genomic architecture of the *Insr* locus across hystricognath species (**Table S3**). Computational cropping of the genomic window between exon 10 and exon 12 revealed a conservation of intron length (ranging between ~ 6.3 kb and ~ 9.4 kb, **Table S4**), ruling out large-scale chromosomal deletions. Instead, high-sensitivity heuristic alignments successfully located the hidden remnants of exon 11 deep within the intronic space of the genus *Cavia*.

Manual inspection of the splicing motifs revealed a complex molecular mechanism of exclusion driven by the degradation of exonic splicing enhancers (ESEs) and the creation of *de novo* exonic splicing silencers (ESSs) (Fig. 5B). In humans, exon 11 inclusion relies on a delicate competitive balance: enhancer proteins (SRp20 and SF2/ASF) bind to the 5' and 3' regions to promote splicing. At the same time, the repressor CUG-BP1 targets the central region to induce exon skipping (Sen et al. 2009).

While caviomorph species (e.g., O*ctodon degus*, *Chinchilla lanigera*, and *Capromys pilorides*) retain robust canonical splicing signals and functional ESE signatures, members of the superfamily Cavioidea (*Hydrochoerus*, *Dolichotis*, and *Cavia*) exhibit marked sequence divergence. Specifically, starting at nucleotide position 13 of the 36-bp exon, the ancestral sequence AGGCAC changed to the highly GC-rich motifs GGGCAG (in *Hydrochoerus* and *Dolichotis*) and CGGTGC (in *Cavia*). This transversional accumulation not only stabilizes a highly repressive stem-loop secondary structure favored by CUG-BP1 (Sen et al. 2009), but also creates a G-rich binding site for hnRNP-F, a known potent silencer of INSR exon 11 (Talukdar et al. 2011).

Furthermore, this functional repression is finalized by downstream loss-of-function mutations. In *Hydrochoerus hydrochaeris* (capybara), the 3' ESE sequence required for SF2/ASF binding (CCCTAG at positions 31–36) was mutated to CTCGAG, destroying the purine-rich motif necessary for spliceosome anchoring (Webster et al. 2004; Sen et al. 2009). Ultimately, the genus *Cavia* (*C. porcellus*, *C. tschudii*, and *C. aperea*) suffered the complete structural degradation of the exon 11 3' splice junction. The strictly required 'GT' dinucleotide at the donor site was mutated into a non-functional 'GG' sequence, physically blinding the spliceosome to this exon and ensuring constitutive skipping. Additionally, advanced pseudogenization was found in the wild relative, *Cavia aperea*, where a 1-bp deletion introduces an unrecoverable reading-frame shift (Fig. 5B). Taken together, these genomic features demonstrate that the loss of INSR-B is not a recent domestication artifact but an ancestral regulatory silencing event that predates the divergence of the species of the *Cavia* clade, likely driven by the altered insulin signaling dynamics characteristic of these rodents (Malakar et al. 2016).

Phylogenetic Mapping and Structural Remodeling of Exon 11

To contextualize the evolutionary trajectory of exon 11 prior to its complete pseudogenization in the genus *Cavia*, we aligned the translated functional protein sequences of this exon across rodents and mapped them directly onto their species phylogeny (**Figure S2**). This coupled visualization of the evolutionary tree and the multiple sequence alignment reveals striking molecular synapomorphies, underscoring a profound functional remodeling of this domain across the histricognath clade. Analysis of the alignment highlights two critical amino acid substitutions that fundamentally alter the biochemistry and electrostatics of the receptor binding interface.

Electrostatic pocket alteration (E→Q): A shift in local electrostatics is observed across the entire clade through the replacement of a negatively charged Glutamic Acid (E) with a neutral Glutamine (Q). This loss of negative charge represents a major disruption of the canonical electrostatic environment at the receptor interface.

Lineage-specific charge neutralization (K→N): Further divergence is observed within specific sub-clades, notably among giant caviomorphs (*Hydrochoerus hydrochaeris* and *Dolichotis patagonum*), African mole-rats (*Fukomys* spp. and *Heterocephalus glaber*), and subterranean tuco-tucos (*Ctenomys* spp.). In these diverse lineages, a positively charged lysine (K) was substituted by a neutral asparagine (N), adding another layer of charge neutralization to the domain. Intriguingly, the degu presents an even more radical

substitution at this exact residue, replacing the positive lysine with a negatively charged glutamic acid (E) (K→E), resulting in a complete charge reversal. Collectively, these parallel signatures demonstrate that even in lineages where exon 11 remains transcriptionally functional, the INSR-B isoform was subjected to significant changes in the properties of some of its amino acids. These widespread, position-specific electrostatic shifts remodel the binding pocket and likely allow the receptor to physically accommodate the highly divergent, biologically atypical insulins characteristic of hystricognath rodents.

Structural Remodeling of the INSR Ectodomain in Ctenomys rionegrensis

To evaluate the three-dimensional and spatial consequences of the sites identified as possibly under positive selection within the hystricognath *INSR*, we generated a full-length *in silico* structural model using AlphaFold3. We selected the subterranean rodent *Ctenomys rionegrensis* as our representative structural model, as its coding sequence was robustly recovered and validated from a *de novo* mixed-tissue transcriptome (incorporating hepatic expression data), thereby ensuring high physiological fidelity of the translated sequence. Superposition of the *C. rionegrensis* structural model against the canonical human insulin receptor structure revealed macroscopic architectural conservation, yet highlighted critical localized deviations at the primary binding interfaces. Specifically, mapping the positively selected residues onto the 3D structure revealed that mutations in the FnIII-1 and β-CT domains are not randomly distributed but rather cluster spatially, thereby modifying the topological and electrostatic landscape of the receptor-binding pockets. Compared with the human INSR, the accumulation of these lineage-specific substitutions in *C. rionegrensis* induces visible steric and conformational shifts at the interfaces classically required to accommodate the canonical insulin molecule. These structural deviations strongly suggest a localized architectural remodeling, possibly driven by positive selection to maintain functional binding affinity with the highly divergent hystricognath insulin (**Figure S3**).

Discussion

Hystricognath rodents represent a compelling natural experiment within the mammalian tree of life. Among their diverse physiological departures, the divergence of the glycemic regulatory axis is the most widely known. Historically, studies have focused on the insulin molecule, which has low metabolic activity, high growth-promoting activity, does not form canonical zinc-hexamers for storage, and is secreted in massive quantities in at least some hystricognaths (Opazo et al. 2005; Irwin 2020; Irwin 2021). Given the tightly integrated functional roles of the insulin signaling pathway, we hypothesized that the receptor (INSR) and its negative regulators (such as ELAPOR1/Inceptor) must have co-evolved to accommodate the divergent insulin molecule. Evidence of positive selection in the insulin gene confirms earlier studies in an expanded data set that includes Old World hystricognaths. We also provide evidence showing that *ELAPOR1*, encoding for Inceptor, has diverged under positive selection in hystricognaths. The evidence for positive selection in the insulin receptor, as revealed by changes in ω, is equivocal: there is strong support for model M8 over M7, but the additional class of amino acid sites in M8 is set at ω = 1, which is consistent with relaxed selective constraints and neutral evolution. However, careful analysis of the evolution of exon 11, whose inclusion characterizes the “long” form of the insulin receptor (INSR-B), typically used for glycemic regulation in canonical mammals, shows that it has undergone significant remodeling among hystricognaths. Furthermore, such remodeling mostly involved silent substitutions that alter splicing and are not captured by analyses based on ω. In the genus *Cavia* (guinea pigs), changes in exon 11 result in its complete ablation, thereby eliminating the INSR-B isoform.

Co-evolution and Structural Remodeling of the Ligand-Receptor Interface

Our analyses confirm that the *Ins* gene underwent intense positive selection across the hystricognath clade. Consistent with previous reports based on narrower taxonomic sampling (Opazo et al. 2005), the adaptive signatures are heavily concentrated at the second binding site (residues A13, B17, B22) and the hexamerization-critical aromatic triplet region (B24–B27). Generalizing, it appears that changes in the second binding site and related sites involved in hexamerization characterize other vertebrates that do not form insulin hexamers (see (Chrudinová et al. 2026).

Results of site models for the *Insr* locus are equivocal: a class of sites with ω ≥ 1 is strongly supported, but ω is set at 1, which is compatible with relaxation of purifying selection in this set of sites. The extreme heterogeneity in how different hystricognath lineages resolved the ligand-receptor incompatibility may explain the failure to detect an unequivocal signal of positive selection on a set of sites across hystricognaths. Just as Opazo et al. (2005) noted varied evolutionary trajectories for the insulin molecule across the clade, our data suggest that Insr did not undergo a single, consistent set of amino acid substitutions across all hystricognaths. Consequently, the statistical signal for classical positive selection (which assumes consistent non-synonymous changes across the phylogeny) is diluted. Sites identified as possibly under positive selection, however, often correspond to insulin-binding amino acids in

the receptor. In addition, and more importantly, our analyses show that the insulin receptor of some lineages of hystricognaths underwent structural remodeling that escapes traditional codon-based evolutionary models. Because ω-based methods solely evaluate rates of non-synonymous changes relative to synonymous changes, they are inherently blind to the regulatory evolution that drove this system, such as synonymous or intronic mutations that destroy splicing enhancer motifs. Lineage-specific neutralization of the binding pocket electrical charges (E→Q and K→N) suggests significant structural changes of the binding interface.

Pseudogenization of exon 11 of INSR

Changes in the region encoded by exon 11 occurred throughout the hystricognath clade. In contrast with mice and rats, which suppress INSR-A and shift to INSR-B in the adult liver (Belfiore et al. 2009), the degu retains the adult expression of INSR-A along with INSR-B, which includes exon 11, albeit one that carries the K→E electrostatic charge reversal. In capybara and guinea pig, only INSR-A is expressed in the adult liver, thus excluding exon 11 from the expressed isoform. The extreme case is the complete pseudogenization of exon 11 in the genus *Cavia*, as shown by a combination of genomic analysis and transcriptomic validation, which reveals the absence of the INSR-B isoform in guinea pig liver. Macroscopically, the intronic architecture of the locus remains conserved, however, a single point mutation at the splice donor site of intron 11 is expected to completely prevent spliceosome recognition. This molecular lesion places the entirety of the hepatic metabolic demand onto INSR-A, an isoform canonically restricted to embryonic development and mitogenic signaling (Choi and Bai 2023). This represents a rare and remarkable evolutionary event, i.e., the resolution of a ligand-receptor incompatibility by permanently disabling the adult metabolic receptor variant. In the biomedical literature, an aberrant shift toward hepatic INSR-A expression is a hallmark of insulin resistance and Type 2 Diabetes, negatively impacting metabolic signaling (Besic et al. 2015). Conversely, in diabetic mouse models, forced hepatic INSR-A expression can act as a basal rescue mechanism by associating with endogenous GLUT transporters (Diaz-Castroverde et al. 2016). Given this scenario, future transcriptomic and physiological studies are warranted to investigate whether downstream elements of glycemic regulation, such as glucose transporters or intracellular kinases like AKT, have also undergone compensatory evolutionary rewiring on the caviomorph clade.

ELAPOR1 as a Potential Compensatory Brake

The systemic consequences of relying solely on the INSR-A isoform, coupled with ectopic hepatic insulin expression, necessitate a robust local mechanism to prevent hyperinsulinemic signaling. The transcriptomic profiling identifies *ELAPOR1* (which encodes for *Inceptor*) as a crucial component of this systemic compensation. Recently characterized as a major negative regulator that promotes clathrin-mediated endocytosis and lysosomal degradation of both insulin and INSR (Ansarullah et al. 2021; Siehler et al. 2024), *ELAPOR1* is overexpressed in the guinea pig liver compared to murine models. Furthermore, we demonstrate that this unique transcriptional profile, characterized by silent *INSR-B*, ectopic *Ins*, and high *ELAPOR1*, is constitutively rigid. In other words, it appears that local expression of *ELAPOR1* is required in tissues that produce insulin, such as the β-cells of the pancreas (Ansarullah et al. 2021; Siehler et al. 2024) or the liver of at least some caviomorphs (e.g., the degu and guinea pig). This proposition is tentative, as *ELAPOR1* is also expressed in the liver of adult laboratory rats (but not mice) with no evidence of local insulin production (**Fig. 5A**).

Limitations and Future Perspectives

Whereas our integrative approach provides compelling evidence for the systemic remodeling of the hystricognath glycemic axis, several limitations inherent to the study of non-model organisms must be acknowledged. First, the reliance on publicly available genomic assemblies of varying quality carries the inherent risk of annotation artifacts or assembly gaps. Although we mitigated this through high-resolution genomic analysis and *de novo* transcriptomic validation in key lineages, the precise evolutionary timing of certain mutations and concomitant changes in expression profiles across the hystricognath clade may require representative genomes across the diversity of hystricognaths, as well as comparative embryonic and adult transcriptomics.

Second, our transcriptomic profiling was primarily focused on hepatic tissues, the primary site of metabolic insulin signaling. The current lack of high-quality pancreatic transcriptomes or single-cell RNA sequencing (scRNA-seq) datasets for the vast majority of hystricognath species limits our ability to fully resolve the *in vivo* expression dynamics of *Ins* and *ELAPOR1* strictly within the pancreatic beta-cells. Future single-cell studies will be crucial to definitively map the synthesis, intracellular regulation, and secretion ratios of these atypical insulins. Finally, our *in silico* structural predictions must be interpreted with caution. Although AlphaFold3 offers state-of-the-art predictive accuracy, modeling the extreme allosteric transition of the insulin receptor remains inherently challenging. The physiological activation of INSR involves massive conformational shifts that are heavily influenced by lipid membrane anchoring and extensive structural glycosylation, dynamic factors not fully captured by static computational algorithms. Consequently,

our 3D models serve primarily as a conceptual visualization tool to support our sequence-level evolutionary findings, rather than a definitive crystallographic resolution of the complex.

The pseudogenization of exon 11 in certain hystricognaths adds an interesting turn to the evolutionary history of the insulin receptor. Exon 11 is typical of mammalian insulin receptors and allows the synthesis of distinct embryonic (INSR-A, lacking exon 11) and adult (INSR-B) receptors, the latter typically characterized by greater insulin specificity (Frasca et al. 1999; Malaguarnera et al. 2012; Jiang et al. 2024). It has recently been documented that exon 11 (or a similar sequence) is also present in turtles and tortoises (Chrudinová et al. 2026), so the evolution of this region of the insulin receptor needs to be re-examined.

Declarations

Acknowledgments

This work was partially supported by a Postdoctoral Fellowship from the Agencia Nacional de Investigación e Innovación (ANII, Uruguay) to Melisa E. Magallanes Alba and matching funds from the Universidad de la República (Uruguay). Juan C. Opazo acknowledges the support of the Fondo Nacional de Desarrollo Científico y Tecnológico of Chile (FONDECYT 1250688).

Author Contributions

Melisa E. Magallanes Alba (MEMA): Conceptualization, Methodology, Software, Formal analysis, Investigation, Data curation, Visualization, Writing – original draft, Writing – review & editing.

Maite Hilario (MH): Formal analysis, Investigation, Data curation, Writing – review & editing.

Juan C. Opazo (JCO): Conceptualization, Methodology, Supervision, Writing – review & editing.

Enrique P. Lessa (EPL): Conceptualization, Resources, Supervision, Project administration, Funding acquisition, Writing – review & editing.

References

1. Abramson J, Adler J, Dunger J, Evans R, Green T, Pritzel A, Ronneberger O, Willmore L, Ballard AJ, Bambrick J, et al. 2024. Accurate structure prediction of biomolecular interactions with AlphaFold 3. *Nature* 630:493–500.
2. Ansarullah, Jain C, Far FF, Homberg S, Wißmiller K, Von Hahn FG, Raducanu A, Schirge S, Sterr M, Bilekova S, et al. 2021. Inceptor counteracts insulin signalling in β-cells to control glycaemia. *Nature* 590:326–331.
3. Bajaj M, Blundell TL, Horuk R, Pitts JE, Wood SP, Gowan LK, Schwabe C, Wollmer A, Gliemann J, Gammeltoft S. 1986. Coypu insulin. Primary structure, conformation and biological properties of a hystricomorph rodent insulin. *Biochemical Journal* 238:345–351.
4. Barbour LA, McCurdy CE, Hernandez TL, Kirwan JP, Catalano PM, Friedman JE. 2007. Cellular Mechanisms for Insulin Resistance in Normal Pregnancy and Gestational Diabetes. *Diabetes Care* 30:S112–S119.
5. Belfiore A, Frasca F, Pandini G, Sciacca L, Vigneri R. 2009. Insulin Receptor Isoforms and Insulin Receptor/Insulin-Like Growth Factor Receptor Hybrids in Physiology and Disease. *Endocrine Reviews* 30:586–623.
6. Besic V, Shi H, Stubbs RS, Hayes MT. 2015. Aberrant Liver Insulin Receptor Isoform A Expression Normalises with Remission of Type 2 Diabetes after Gastric Bypass Surgery.Sanchez-Margalet V, editor. *PLoS ONE* 10:e0119270.
7. Bilekova S, Garcia-Colomer B, Cebrian-Serrano A, Schirge S, Krey K, Sterr M, Kurth T, Hauck SM, Lickert H. 2023. Inceptor facilitates acrosomal vesicle formation in spermatids and is required for male fertility. *Front. Cell Dev. Biol.* 11:1240039.
8. Blundell TL, Dodson GG, Dodson E, Hodgkin DC, Vijayan M. 1971. X-Ray Analysis and the Structure of Insulin. In: Proceedings of the 1970 Laurentian Hormone Conference. Elsevier. p. 1–40. Available from: https://linkinghub.elsevier.com/retrieve/pii/B9780125711272500250
9. Bray NL, Pimentel H, Melsted P, Pachter L. 2016. Near-optimal probabilistic RNA-seq quantification. *Nat Biotechnol* 34:525–527.
10. Burchfield JG, James DE. 2021. A co-receptor that represses beta-cell insulin action. *Nat Metab* 3:126–127.
11. Choi E, Bai X-C. 2023. The Activation Mechanism of the Insulin Receptor: A Structural Perspective. *Annu. Rev. Biochem.* 92:247–272.

12. Chrudinová M, DaCosta JM, Dogru D, Huang R, Reiners R, De Meyts P, Altindis E. 2026. Evolution of Insulin, Insulin-like Growth Factors, and Their Cognate Receptors in Vertebrates, Invertebrates, and Viruses.Ozkan B, editor. *Molecular Biology and Evolution* 43:msaf319.
13. Conlon JM. 2001. Evolution of the insulin molecule: insights into structure-activity and phylogenetic relationships. *Peptides* 22:1183–1193.
14. Davidson JK, Haist RE. 1965. FAILURE OF GUINEA PIG ANTIBODY TO BEEF INSULIN TO NEUTRALIZE PANCREATIC AND SERUM GUINEA PIG INSULIN ACTIVITY IN VITRO. *Can. J. Physiol. Pharmacol.* 43:373–378.
15. Davidson JK, Zeigle M, Haist RE. 1968. Failure of Guinea Pig Antibody to Beef Insulin to Neutralize Coypu (Nutria) Insulin. *Diabetes* 17:8–12.
16. De Meyts P. 2015. Insulin/receptor binding: The last piece of the puzzle?: What recent progress on the structure of the insulin/receptor complex tells us (or not) about negative cooperativity and activation. *BioEssays* 37:389–397.
17. D'Elía G, Fabre P-H, Lessa EP. 2019. Rodent systematics in an age of discovery: recent advances and prospects. *Journal of Mammalogy* 100:852–871.
18. Diaz-Castroverde S, Gómez-Hernández A, Fernández S, García-Gómez G, Di Scala M, González-Aseguinolaza G, Fernández-Millán E, González-Rodríguez Á, García-Bravo M, Chambon P, et al. 2016. Insulin receptor isoform A ameliorates long-term glucose intolerance in diabetic mice. *Disease Models & Mechanisms* 9:1271–1281.
19. Edwards MS. 2009. Nutrition and Behavior of Degus (Octodon degus). *Veterinary Clinics of North America: Exotic Animal Practice* 12:237–253.
20. Frasca F, Pandini G, Scalia P, Sciacca L, Mineo R, Costantino A, Goldfine ID, Belfiore A, Vigneri R. 1999. Insulin Receptor Isoform A, a Newly Recognized, High-Affinity Insulin-Like Growth Factor II Receptor in Fetal and Cancer Cells. *Mol Cell Biol* 19:3278–3288.
21. Gutmann T, Schäfer IB, Poojari C, Brankatschk B, Vattulainen I, Strauss M, Coskun Ü. 2020a. Cryo-EM structure of the complete and ligand-saturated insulin receptor ectodomain. *Journal of Cell Biology* 219:e201907210.
22. Gutmann T, Schäfer IB, Poojari C, Brankatschk B, Vattulainen I, Strauss M, Coskun Ü. 2020b. Cryo-EM structure of the complete and ligand-saturated insulin receptor ectodomain. *Journal of Cell Biology* 219:e201907210.
23. Haig D. 1993. Genetic Conflicts in Human Pregnancy. *The Quarterly Review of Biology* 68:495–532.
24. Hall C, Choi E. 2021. New scavenger to fine-tune insulin action in β cells. *Cell Metabolism* 33:707–708.
25. Hasan D, Bionaz M, Kutzler M, Patton K. 2025. Comparative RNA-seq analysis of fetal and maternal guinea pig liver transcriptomes reveals widespread transcriptional divergence. :7086233218 Bytes. Available from: https://figshare.com/articles/dataset/Comparative_RNA-seq_analysis_of_fetal_and_maternal_guinea_pig_liver_transcriptomes_reveals_widespread_transcriptional_divergence_/30570161
26. Herrera-Álvarez S, Karlsson E, Ryder OA, Lindblad-Toh K, Crawford AJ. 2021. How to Make a Rodent Giant: Genomic Basis and Tradeoffs of Gigantism in the Capybara, the World's Largest Rodent.Rogers R, editor. *Molecular Biology and Evolution* 38:1715–1730.
27. Horuk R, Goodwin P, O'Connor K, Neville RWJ, Lazarus NR, Stone D. 1979. Evolutionary change in the insulin receptors of hystricomorph rodents. *Nature* 279:439–440.
28. Irwin DM. 2020. Variation in the rates of evolution of the insulin and glucagon hormone and receptor genes in rodents. *Gene* 728:144296.
29. Irwin DM. 2021. Evolution of the mammalian insulin (Ins) gene; Changes in proteolytic processing. *Peptides* 135:170435.
30. Jiang M, Wang N, Zhang Y, Zhang J, Li Y, Yan X, Zhang H, Li C, Guan Y, Liang B, et al. 2024. Insulin receptor isoform B is required for efficient proinsulin processing in pancreatic β cells. *iScience* 27:110017.
31. Jin Chan S, Steiner DF. 2000. Insulin Through the Ages: Phylogeny of a Growth Promoting and Metabolic Regulatory Hormone. *Am Zool* 40:213–222.
32. Kim D, Langmead B, Salzberg SL. 2015. HISAT: a fast spliced aligner with low memory requirements. *Nat Methods* 12:357–360.
33. King GL, Kahn CR. 1981. Non-parallel evolution of metabolic and growth-promoting functions of insulin. *Nature* 292:644–646.
34. King GL, Kahn CR, Heldin CH. 1983. Sharing of biological effect and receptors between guinea pig insulin and platelet-derived growth factor. *Proc. Natl. Acad. Sci. U.S.A.* 80:1308–1312.
35. Lawrence MC. 2021. Understanding insulin and its receptor from their three-dimensional structures. *Molecular Metabolism* 52:101255.

36. Li H. 2023. Protein-to-genome alignment with miniprot.Valencia A, editor. *Bioinformatics* 39:btad014.
37. Lu JY, Simon M, Zhao Y, Ablaeva J, Corson N, Choi Y, Yamada KYH, Schork NJ, Hood WR, Hill GE, et al. 2022. Comparative transcriptomics reveals circadian and pluripotency networks as two pillars of longevity regulation. *Cell Metabolism* 34:836-856.e5.
38. Malaguarnera R, Sacco A, Voci C, Pandini G, Vigneri R, Belfiore A. 2012. Proinsulin Binds with High Affinity the Insulin Receptor Isoform A and Predominantly Activates the Mitogenic Pathway. *Endocrinology* 153:2152–2163.
39. Malakar P, Chartarifsky L, Hija A, Leibowitz G, Glaser B, Dor Y, Karni R. 2016. Insulin receptor alternative splicing is regulated by insulin signaling and modulates beta cell survival. *Sci Rep* 6:31222.
40. Meng EC, Goddard TD, Pettersen EF, Couch GS, Pearson ZJ, Morris JH, Ferrin TE. 2023. UCSF ChimeraX : Tools for structure building and analysis. *Protein Science* 32:e4792.
41. Napso T, Yong HEJ, Lopez-Tello J, Sferruzzi-Perri AN. 2018. The Role of Placental Hormones in Mediating Maternal Adaptations to Support Pregnancy and Lactation. *Front. Physiol.* 9:1091.
42. Neville RWJ, Weir BJ, Lazarus NR. 1973. Insulins of Hystricomorph Rodents. *Diabetes* 22:851–853.
43. O'Leary NA, Cox E, Holmes JB, Anderson WR, Falk R, Hem V, Tsuchiya MTN, Schuler GD, Zhang X, Torcivia J, et al. 2024. Exploring and retrieving sequence and metadata for species across the tree of life with NCBI Datasets. *Sci Data* 11:732.
44. Opazo JC, Palma RE, Melo F, Lessa EP. 2005. Adaptive Evolution of the Insulin Gene in Caviomorph Rodents. *Molecular Biology and Evolution* 22:1290–1298.
45. Opazo JC, Soto-Gamboa M, Bozinovic F. 2004. Blood glucose concentration in caviomorph rodents. *Comparative Biochemistry and Physiology Part A: Molecular & Integrative Physiology* 137:57–64.
46. Paradis E, Schliep K. 2019. ape 5.0: an environment for modern phylogenetics and evolutionary analyses in R.Schwartz R, editor. *Bioinformatics* 35:526–528.
47. Pertea G, Pertea M. 2020. GFF Utilities: GffRead and GffCompare. *F1000Res* 9:304.
48. Prjibelski A, Antipov D, Meleshko D, Lapidus A, Korobeynikov A. 2020. Using SPAdes De Novo Assembler. *CP in Bioinformatics* 70:e102.
49. Ranwez V, Chantret N, Delsuc F. 2021. Aligning Protein-Coding Nucleotide Sequences with MACSE. In: Katoh K, editor. Multiple Sequence Alignment. Vol. 2231. Methods in Molecular Biology. New York, NY: Springer US. p. 51–70. Available from: http://link.springer.com/10.1007/978-1-0716-1036-7_4
50. Robinson JT, Thorvaldsdóttir H, Winckler W, Guttman M, Lander ES, Getz G, Mesirov JP. 2011. Integrative genomics viewer. *Nat Biotechnol* 29:24–26.
51. Rostène W, De Meyts P. 2021. Insulin: A 100-Year-Old Discovery With a Fascinating History. *Endocrine Reviews* 42:503–527.
52. Sayers EW, Bolton EE, Brister JR, Canese K, Chan J, Comeau DC, Connor R, Funk K, Kelly C, Kim S, et al. 2022. Database resources of the national center for biotechnology information. *Nucleic Acids Res* 50:D20–D26.
53. Seino S, Bell GI. 1989. Alternative splicing of human insulin receptor messenger RNA. *Biochemical and Biophysical Research Communications* 159:312–316.
54. Sen S, Talukdar I, Webster NJG. 2009. SRp20 and CUG-BP1 Modulate Insulin Receptor Exon 11 Alternative Splicing. *Molecular and Cellular Biology* 29:871–880.
55. Siehler J, Bilekova S, Chapouton P, Dema A, Albanese P, Tamara S, Jain C, Sterr M, Enos SJ, Chen C, et al. 2024. Inceptor binds to and directs insulin towards lysosomal degradation in β cells. *Nat Metab* 6:2374–2390.
56. Slater GSC, Birney E. 2005. Automated generation of heuristics for biological sequence comparison. *BMC Bioinformatics* 6:31.
57. Talukdar I, Sen S, Urbano R, Thompson J, Yates JR, Webster NJG. 2011. hnRNP A1 and hnRNP F Modulate the Alternative Splicing of Exon 11 of the Insulin Receptor Gene.Zheng Z-M, editor. *PLoS ONE* 6:e27869.
58. Upham NS, Esselstyn JA, Jetz W. 2019. Inferring the mammal tree: Species-level sets of phylogenies for questions in ecology, evolution, and conservation.Tanentzap AJ, editor. *PLoS Biol* 17:e3000494.
59. Verta J-P, Jacobs A. 2022. The role of alternative splicing in adaptation and evolution. *Trends in Ecology & Evolution* 37:299–308.
60. Webster NJ, Evans L-G, Caples M, Erker L, Chew SL. 2004. Assembly of splicing complexes on exon 11 of the human insulin receptor gene does not correlate with splicing efficiency in-vitro. *BMC Molecular Biol* 5:7.
61. Weiss MA, Lawrence MC. 2018. A thing of beauty: Structure and function of insulin's "aromatic triplet." *Diabetes Obesity Metabolism* 20:51–63.

62. Wood SP, Blundell TL, Wollmer A, Lazarus NR, Neville RWJ. 1975. The Relation of Conformation and Association of Insulin to Receptor Binding; X-Ray and Circular-Dichroism Studies on Bovine and Hystricomorph Insulins. *European Journal of Biochemistry* 55:531–542.
63. Yang Z. 2007. PAML 4: Phylogenetic analysis by maximum likelihood. *Molecular Biology and Evolution* 24:1586–1591.
64. Zimmerman AE, Moule ML, Yip CC. 1974. Guinea Pig Insulin. *Journal of Biological Chemistry* 249:4026–4029.

Table

Table 1 is available in the supplementary files section

Figures

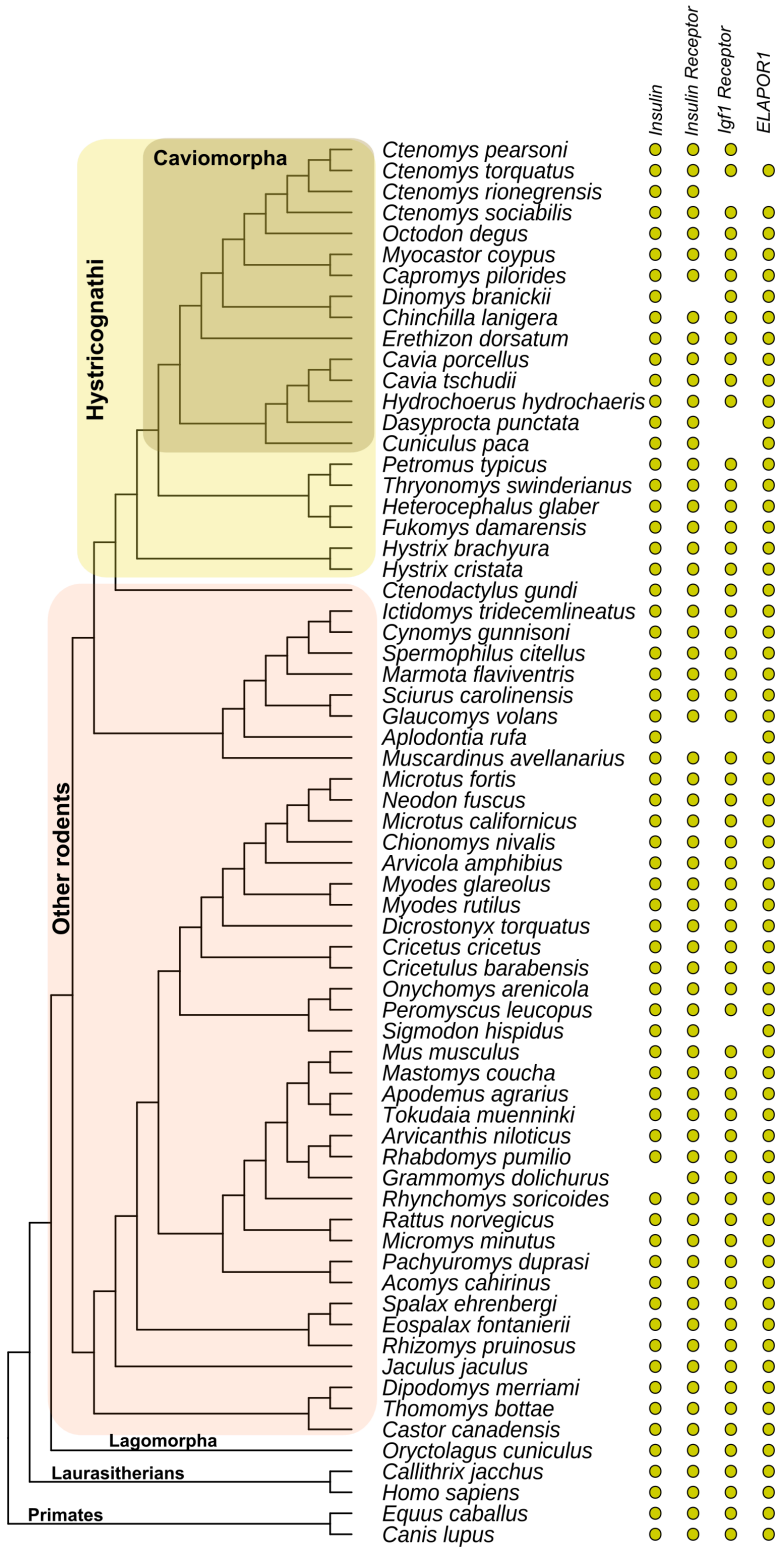


Figure 1

Phylogenetic relationships of the species included in this study. The tree topology is a majority-rule consensus of 1000 trees sampled from the VertLife database (https://vertlife.org/data/mammals), which provides a posterior distribution of species-level phylogenetic trees for mammals inferred under a Bayesian framework integrating molecular sequence data and taxonomic constraints (Upham et al., 2019). IGF1 Receptor: Insulin-like growth factor 1 receptor; ELAPOR1: Endosome-Lysosome Associated Apoptosis and Autophagy Regulator 1. The dots indicate the species representation for each locus.

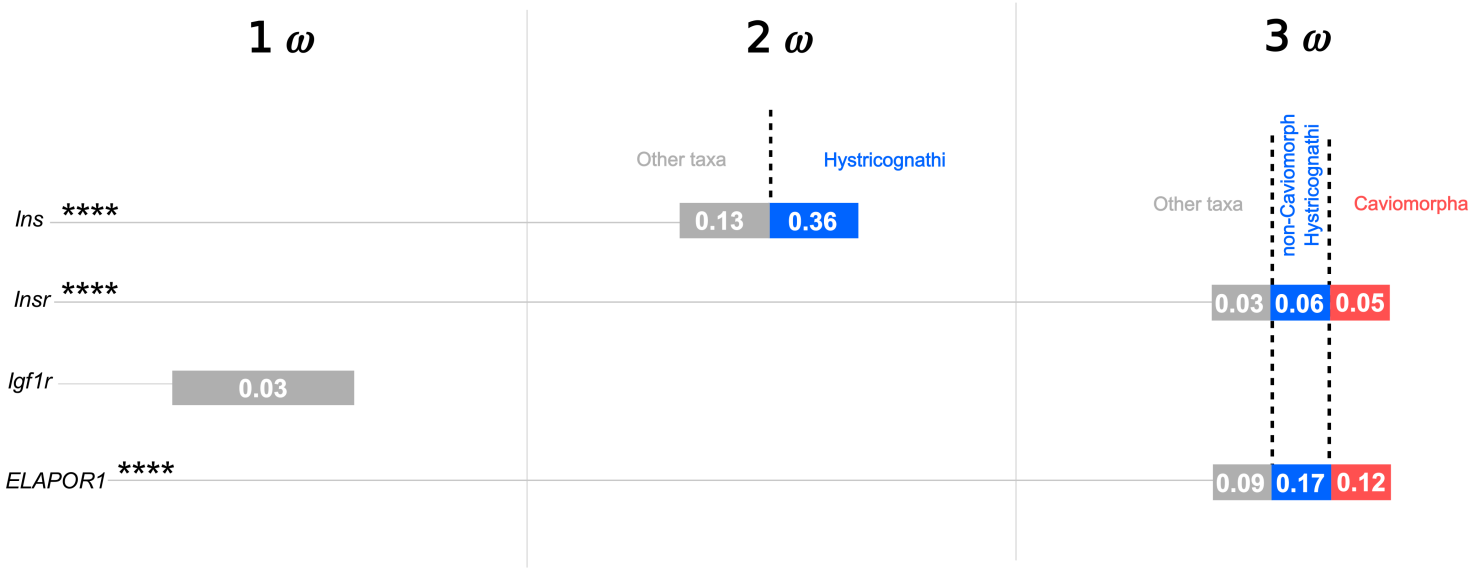


Figure 2

Branch-model estimates of ω (= d_N/d_S) across lineages for the four genes analyzed.

ω ratios were estimated in CODEML under models allowing one (1ω), two (2ω), or three (3ω) distinct nonsynonymous/synonymous substitution rate ratios, corresponding respectively to (i) a single ω across all branches, (ii) separate ω for hystricognath rodents versus other mammals, and (iii) distinct ωs for other taxa, non-caviomorph hystricognaths, and caviomorph lineages (see Fig. 1). The values shown correspond to the best-fitting model for each gene: two-rate model for Ins, three-rate model for *Insr* and *ELAPOR1*, and one-rate (null) model for *Igf1r*. Asterisks denote significant likelihood ratio tests (LRTs) between nested models (***$p < 0.0001$).

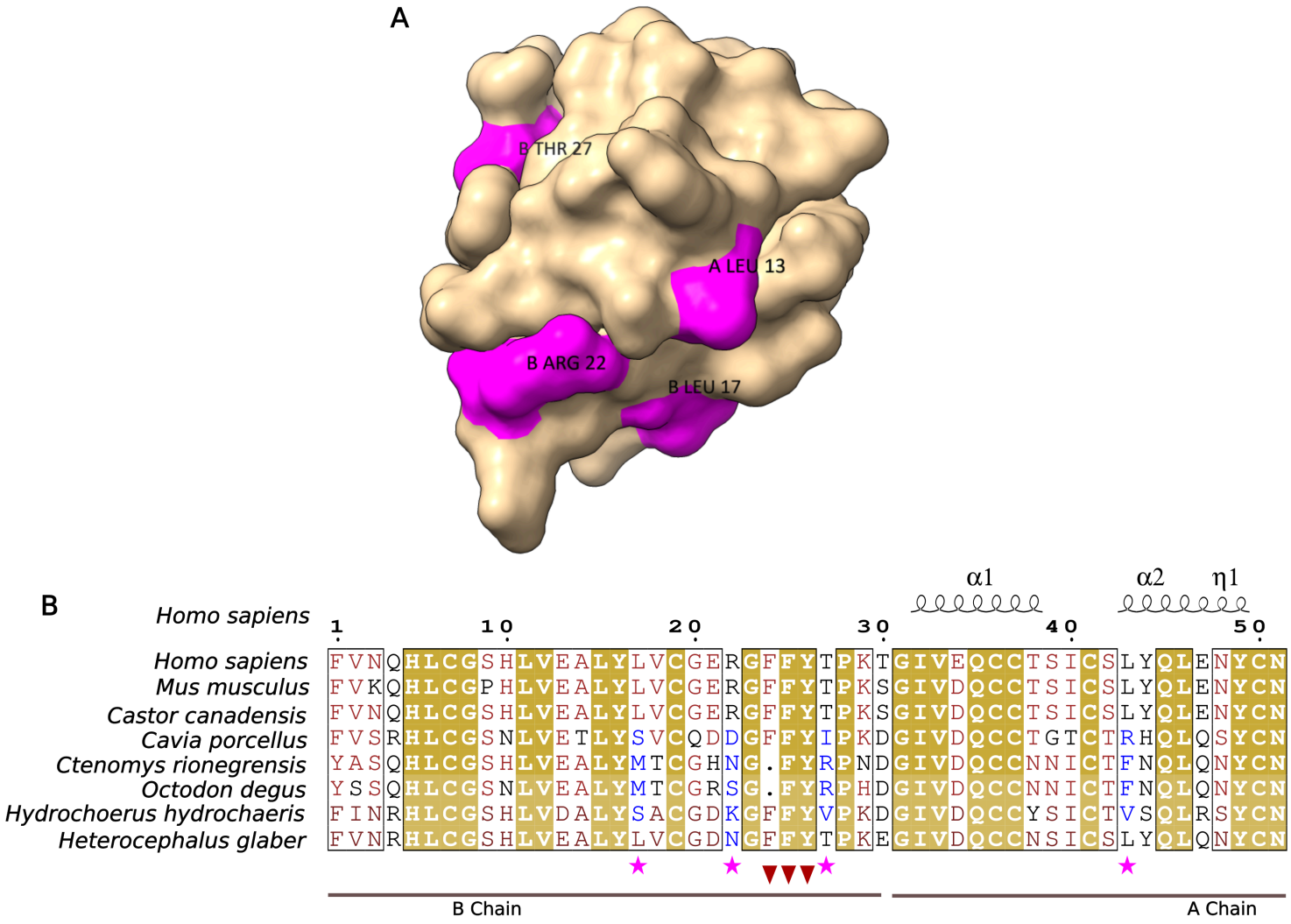


Figure 3

Structural mapping and sequence divergence of positively selected sites in hystricognath insulin. (A) Surface representation of the mature canonical insulin monomer (PDB: 4INS) generated using UCSF ChimeraX. Residues identified to be under positive selection in the hystricognath lineage are highlighted in magenta. Positions A13, B17, and B22 cluster tightly in 3D space and map directly onto the classical "site 2" interface, which is critical for both receptor interaction and hexamerization. Position B27 is located adjacent to the dimerization interface. Position B22 was reported under positive selection in Opazo et al. (2005) and is marginal (PP = xx) in this study.

(B) Multiple sequence alignment of the mature insulin B and A chains, comparing non-hystricognath mammals with representative hystricognath rodents. Secondary structure elements (α-helices) derived from the PDB structure (INS) are displayed above the alignment. The positively selected sites are marked with magenta stars, illustrating lineage-specific amino acid substitutions relative to the highly conserved canonical sequences. The classical "aromatic triplet" (B24–B26), an essential structural motif for receptor binding and hexamer formation, is outlined in blue triangles, highlighting its structural degradation and the loss of aromaticity across the hystricognath clade.

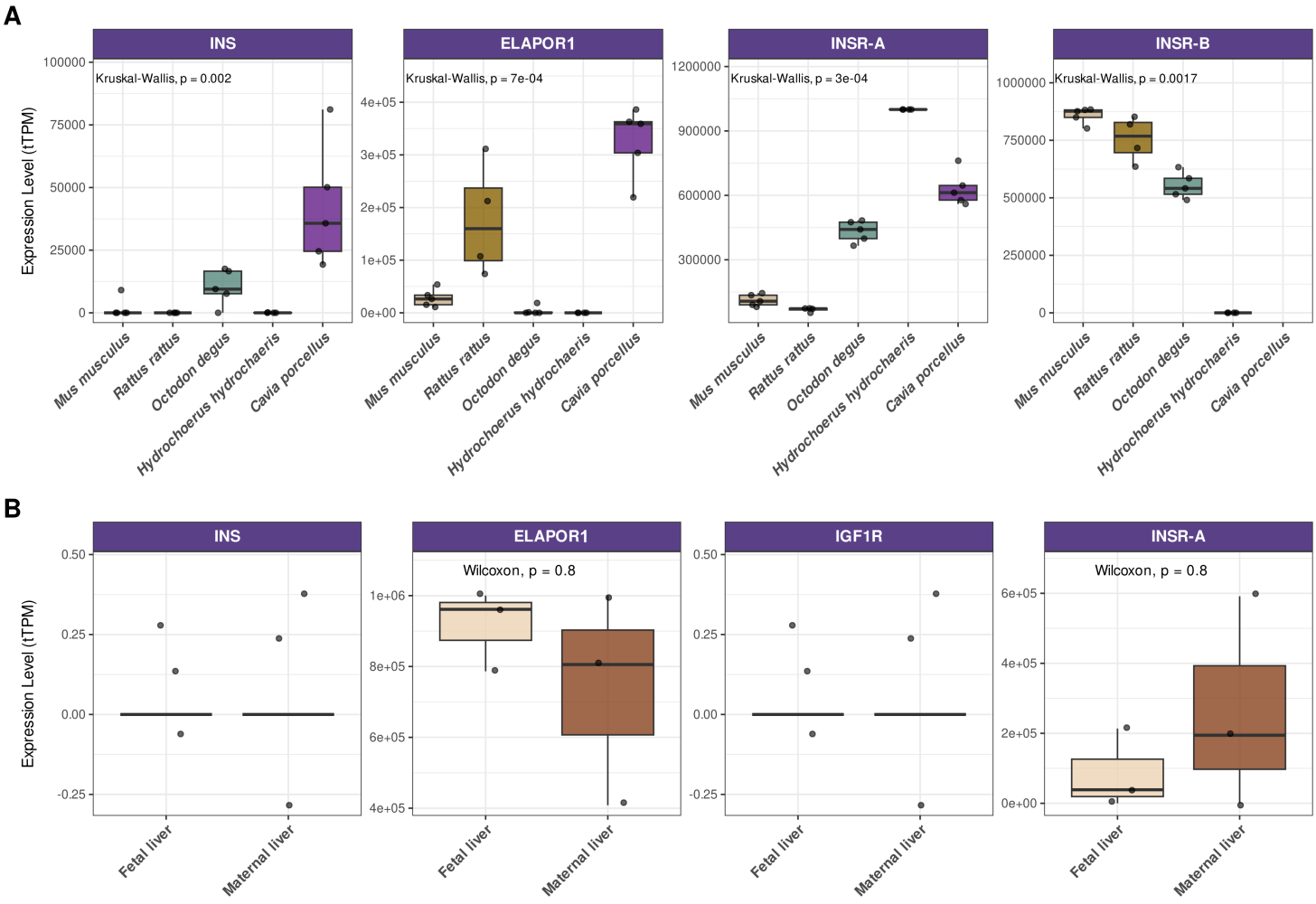


Figure 4

Transcriptomic profiling of the systemic compensatory response in the livers of the guinea pig (*C. porcellus*) and degu (*O. degus*) under physiological and stress conditions.Expression levels are reported as targeted Transcripts Per Million (tTPM). **(A)**Expression levels of components of the insulin signaling axis in healthy adult *C. porcellus* and *O. degus* compared with murine models. **(B)** Comparison of transcript abundance between fetal and maternal liver tissues in guinea pigs.

Image not available with this version

Figure 5

Physical validation of exon 11 skipping in the guinea pig*INSR* transcript. **(A)** RNA-seq read coverage and a Sashimi plot illustrating splicing dynamics across exons 8-13 of the hepatic insulin receptor. The bottom track displays the genomic coordinates and the reconstructed structural model of the *INSR* locus. The theoretical genomic position of the alternatively spliced exon 11 is highlighted in red. The coverage track is indicated by the blue histogram and the Sashimi arcs in orange.

(B) Nucleotide alignment of the genomic locus encompassing exon 11. Vertical lines explicitly demarcate the boundaries between intron 10, exon 11, and intron 11. Splice acceptor site and splice donor sites flanking exon 11 are indicated in bold; point substitutions are highlighted in red. SRp20, CUG-BP1, and SF2/ASF indicate.

Supplementary Files

This is a list of supplementary files associated with this preprint. Click to download.

- Table1.xlsx
- TableS1.xlsx
- TableS2.xlsx
- TableS3.xlsx
- TableS4.xlsx
- FigureS1.png
- FigureS2.png
- FigureS3.png